RESEARCH ARTICLE

WILEY

Driving brain state transitions in major depressive disorder through external stimulation

Shengpei Wang[1] | **Hongwei Wen[2,3]** | **Shuang Qiu[1]** | **Peng Xie[4,5,6]** | **Jiang Qiu[2,3]** | **Huiguang He[1,7,8]**

[1]Research Centre for Brain-inspired Intelligence and National Laboratory of Pattern Recognition, Institute of Automation, Chinese Academy of Sciences, Beijing, China

[2]Key Laboratory of Cognition and Personality (Ministry of Education), Chongqing, China

[3]School of Psychology, Southwest University, Chongqing, China

[4]Institute of Neuroscience, Chongqing Medical University, Chongqing, China

[5]Chongqing Key Laboratory of Neurobiology, Chongqing, China

[6]Department of Neurology, the First Affiliated Hospital of Chongqing Medical University, Chongqing, China

[7]University of Chinese Academy of Sciences, Beijing, China

[8]Center for Excellence in Brain Science and Intelligence Technology, Chinese Academy of Sciences, Beijing, China

Correspondence
Jiang Qiu, Key Laboratory of Cognition and Personality (Ministry of Education), School of Psychology, Southwest University, Tiansheng Road 2#, Chongqing 400715, China.
Email: qiuj318@swu.edu.cn

Huiguang He, Research Center for Brain-inspired Intelligence and National Laboratory of Pattern Recognition, Institute of Automation, Chinese Academy of Sciences, Zhongguancun East Road. 95#, Beijing 100190, China.
Email: huiguang.he@ia.ac.cn

Abstract

Major depressive disorder (MDD) as a dysfunction of neural circuits and brain networks has been established in modern neuroimaging sciences. However, the brain state transitions between MDD and health through external stimulation remain unclear, which limits translation to clinical contexts and demonstrable clinical utility. We propose a framework of the large-scale whole-brain network model for MDD linking the underlying anatomical connectivity with functional dynamics obtained from diffusion tensor imaging (DTI) and functional magnetic resonance imaging (fMRI). Then, we further explored the optimal brain regions to promote the transition of brain states between MDD and health through external stimulation of the model. Based on the whole-brain model successfully fitting the brain state space in MDD and the health, we demonstrated that the transition from MDD to health is achieved by the excitatory activation of the limbic system and from health to MDD by the inhibitory stimulation of the reward circuit. Our finding provides novel biophysical evidence for the neural mechanism of MDD and its recovery and allows the discovery of new stimulation targets for MDD recovery.

KEYWORDS
brain state transitions, excitatory stimulation, functional dynamics, major depressive disorder, whole-brain model

---

Shengpei Wang and Hongwei Wen should be considered as co-first authors.

1 | INTRODUCTION

Individuals can be devastated by neuropsychiatric diseases, which are an increasing and major health burden for society. With a lifetime prevalence of 17%, major depressive disorder (MDD) is the main cause of years lost to disability worldwide, and it is expected to be the leading contributor to the global burden of illness by 2030 (Geneva: World Health Organization, 2008; Hock et al., 2012). Benefiting from modern neuroimaging techniques, new findings regarding the structure and function of the human brain provide the most direct information for understanding the neurological mechanisms of mood disorders (Delvecchio et al., 2020; Yan et al., 2019; Zhang et al., 2018; Zhuo et al., 2019). For example, a recent study using the REST-meta-MDD Consortium dataset (which included 1300 patients with depression and 1128 healthy controls from 25 cohorts in China) discovered that decreased functional connectivity (FC) of the default mode network (DMN) in MDD patients was a potential biomarker linked to symptom severity and current medication treatment. This finding suggests that the dysfunction connectivity of DMN remains a prime target for understanding the pathophysiology of depression, with particular relevance to revealing the mechanisms of effective treatments (Yan et al., 2019). Therefore, advances from modern neuroimaging sciences suggest excellent potential as reliable indices to aid in the diagnosis and treatment planning of MDD (Woo et al., 2017).

Based on network science, the brain system, as well as its interactions with other complex systems, may be described by the mathematical theory of graphs (Bullmore & Sporns, 2009; den Heuvel et al., 2010; den Heuvel et al., 2013). By generating the detailed structural and functional maps of the human brain network, we can sketch the network architecture underlying and enabling cognition and further identify their alterations in neurological and psychiatric disorders (Bassett & Bullmore, 2009; Fornito & Bullmore, 2015; Medaglia et al., 2015; Petersen & Sporns, 2015). Numerous studies based on network science provided exciting new insights into disrupted network structures of the human brain for MDD and further suggested network analysis has emerged as a highly promising approach for probing the underlying biological mechanisms of MDD (Ma et al., 2020; Nixon et al., 2014; Yang et al., 2021). Recent reviews suggest that abnormal communication within and between brain structural and functional networks underscores the complex psychopathology observed in MDD (Brakowski et al., 2017; Dai et al., 2019; Dunlop et al., 2019; Kerestes et al., 2014; Nixon et al., 2014). Particularly, the connectivity of limbic structures, salience network, DMN, and central executive network (CEN) give rise to diverse domains of abnormal behavior, including rumination, cognitive control deficits, and anhedonia in MDD. Additionally, the latest study from 16 cohorts regarding MDD observed the disrupted topological structure of functional brain networks in MDD, suggesting decreased brain network efficiency locally and globally (Yang et al., 2021). Despite substantial evidence have indicated that MDD can be characterized as dysfunctions of circuits and networks of the human brain (Bora et al., 2012; Rubinov & Bullmore, 2013; Yang et al., 2021), the

translation of these findings to clinical contexts and demonstrable clinical utility is still in its infancy. One of the major challenges stems partly from the fact that the current approaches are largely descriptive and lack a mechanistic account of the circuit function of the human brain (Braun et al., 2018). And addressing this challenge is critical for the prospective development of interventions and treatments for depressive disorders and even for enhancing cognitive function in psychiatric disorders.

Inspired by the success of modern physics, the mechanistic whole-brain model of the underlying brain dynamics seems to have emerged as a possible way to overcome this challenge (Deco, Ponce-Alvarez, et al., 2014; Demirtaş et al., 2019; Ghosh et al., 2008; Kringelbach et al., 2020; Kringelbach & Deco, 2020). Linking anatomical structures with functional dynamics, the whole-brain model can simulate brain dynamics to discover the mechanistic principles of the human brain in both health and disorder. Recent studies have indicated that the whole-brain model successfully explains the patterns of spontaneous interregional functional activity correlations (Breakspear, 2004; Deco et al., 2010; Deco, McIntosh, et al., 2014). Meanwhile, these enhanced descriptions of brain activity are not only useful for understanding the human healthy brain but have great potential to help support diagnosis and therapeutic interventions in disease states (Deco & Kringelbach, 2014; Gilson et al., 2020). The whole-brain model has proven to be useful for clinical conditions of neurological and psychiatric disorders, such as stroke (Adhikari et al., 2017), epilepsy (Hashemi et al., 2020), and brain tumors (Aerts et al., 2020). It is more noteworthy that the whole-brain model can be used to probe how the input affects neural dynamics, which would allow for the potential prediction of interventions to rebalance diseased brain states (Deco et al., 2019; Kringelbach & Deco, 2020). Recent studies adopted the whole-brain model to fit the probabilistic metastable substate (PMS) space of the two radically different brain states of human sleep and wakefulness and then to investigate the most suitable stimulation of this whole-brain model to force transitions between different brain states (Deco et al., 2019). Therefore, the whole-brain model will allow us to address a fundamental question regarding how brain transitions occur between health and depressive disorders.

Here, we propose a simple framework of the whole-brain network in MDD linking the underlying anatomical connectivity with functional dynamics obtained from diffusion tensor imaging (DTI) and functional magnetic resonance imaging (fMRI). We constructed a structural brain network based on DTI, in which nodes represented the region of the anatomical automatic labeling (AAL) atlas, and edges represented quantitative anisotropy between these regions estimated from diffusion tractography. Based on this structural network, we built a large-scale whole-brain model with a dynamic mean-field (DMF) model, optimized to successfully fit the respective brain state space of the health and MDD defined by fMRI. Finally, using the whole-brain model, we probed the optimal brain regions to promote the transition of brain states between participants with MDD and healthy controls through excitatory or inhibitory external stimulation of the whole-brain dynamic model.

2 | MATERIALS AND METHODS

2.1 | Participants and MRI acquisition

One hundred twenty-seven participants with MDD (83 females and 44 males, mean age, 38.32 ± 13.76 years, age range, 12–74 years) and 117 age- and sex-matched healthy participants (74 females and 43 males, mean age, 38.89 ± 14.14 years, range, 19–72 years) were recruited from the First Affiliated Hospital of Chongqing Medical School. All subjects independently underwent a diagnostic interview conducted by experienced psychiatrists according to the Structured Clinical Interview for the Diagnostic and Statistical Manual of Mental Disorders, 2nd edition, for Axis I Disorders. The main exclusion criteria were derived from previous studies (Cheng, Rolls, Qiu, Yang, et al., 2018; Wei et al., 2019). Depression severity was rated using the Hamilton Depression Scale and Hamilton Anxiety Scale by interview and self-report scales in the Beck Depression Inventory-II. Additionally, our study design was approved by the Institutional Review Board of Chongqing Medical University and performed in accordance with the principles of the Declaration of Helsinki. Written informed consent was obtained from all participants.

2.2 | Structural and functional MRI acquisition

Structural and functional MRI images were acquired on a 3 T Siemens Trio MRI scanner using a 12-channel whole-brain coil (Siemens Medical, Erlangen, Germany) in the First Affiliated Hospital of Chongqing Medical School. Diffusion tensor imaging (DTI), high-resolution 3D T1-weighted image, and resting-state fMRI were acquired for each participant. DTI data were acquired with spin-echo diffusion-weighted echo-planar imaging with the following parameters: repetition time (TR) = 11,000 ms, echo time (TE) = 98 ms, inversion time = 900 ms, reconstructed image matrix = 128 × 124, field of view (FOV) = 256 × 248 mm^2, slice thickness = 2 mm with no interslice gap, voxel size = 2 × 2 × 2 mm^2, 60 axial slices. Diffusion MRI images were obtained from 61 noncollinear directions with a b value of 1000 s/mm^2 and an additional image without diffusion weighting (i.e., b = 0 s/mm^2). High-resolution 3D T1-weighted imaging were acquired using magnetization-prepared rapid acquisition gradient-echo sequence (MPRAGE) with the following parameters: TR = 1900 ms, TE = 2.52 ms, inversion time = 900 ms, flip angle = 9°, reconstructed image matrix = 256 × 256, FOV = 200 × 200 mm^2, 176 axial slices; slice thickness = 1 mm; voxel size = 1 × 1 × 1 mm^3. Resting-state fMRI was acquired using an echo-planar imaging (EPI) sequence with the following parameters: TR = 2000 ms; TE = 30 ms; flip angle = 90°; reconstructed matrix = 64 × 64; FOV = 220 × 220 mm^2. The 32 axial slices; slice thickness = 3 mm; voxel size = 3 × 3 × 3 mm^3, 242 volumes lasting for 484 s. During scanning, participants were instructed to keep their eyes closed, relax, and move as little as possible.

2.3 | Structural and functional MRI processing

Preprocessing of DTI and resting-state fMRI data was performed according to the standard preprocessing steps. In particular, DTI data processing was carried out using the FMRIB's Diffusion Toolbox (FDT 2.0) with FSL v4.1 (http://www.fmrib.ox.ac.uk/fsl). The default parameters of this imaging preprocessing pipeline were used for all participants. Then, structural connectivity maps or structural brain networks were generated for each participant involving the following step: (1) regions of the whole-brain network were defined using the AAL atlas (considering only the 90 cortical and subcortical noncerebellar brain regions), as used in the resting-sate fMRI; (2) probabilistic tractography was used to estimate the connections between regions of the whole-brain network; (3) three group-averaged structural connectivity maps were respectively obtained across all subjects, across all MDD participants, and across the healthy controls.

Meanwhile, resting-state fMRI data preprocessing was performed using statistical parametric mapping (SPM8) (https://www.fil.ion.ucl.ac.uk/spm/) and Data Processing & Analysis for Resting-state Brain Imaging (DPABI) (http://rfmri.org/dpabi) (Yan et al., 2016). The preprocessing steps included the following steps: (1) removing the first 10 time points; (2) temporal and head motion correction; (3) normalization to the standard space of Montreal Neurological Institute (MNI); (4) spatial smoothing using Gaussian kernel with a full width at half maximum = 4 mm; (5) temporally band-pass filtering with 0.01–0.08 Hz; (6) regressing out nuisance signals (including 24-parameter head-motion profiles, mean white matter [WM], and cerebrospinal fluid [CSF] time series). Finally, the averaged blood-oxygenation-level-dependent (BOLD) time series from 90 regions of interest (ROIs) were extracted using the AAL atlas.

2.4 | Leading eigenvector dynamics analysis

To capture the amount of interregional BOLD signal synchrony at any given time point, we first extracted the averaged BOLD time series from all voxels within regions defined in the AAL atlas for all participants (including 127 MDDs and 117 healthy controls), and Hilbert transformed the averaged BOLD time series to yield the phase evolution of the regional signals (Figure 1a). Then, a time-resolved dynamic FC matrix was defined using the BOLD phase coherence connectivity, and the corresponding time-resolved leading eigenvector across time points and subjects (including 232-time points for each subject) was computed. The time-resolved leading eigenvector can capture the dominant connectivity pattern of the dynamic FC matrix at a given time (Figure 1b). In particular, the phase coherence connectivity between each pair of brain regions is given by (Deco et al., 2019):

$$dFC(i,j,t) = \cos(\theta(i,t) - \theta(j,t)) \tag{1}$$

where the BOLD phase $\theta(i,t)$ at a region i is estimated using the Hilbert transform for each regional BOLD time series. In addition, the leading eigenvector at each time point was calculated to reduce the
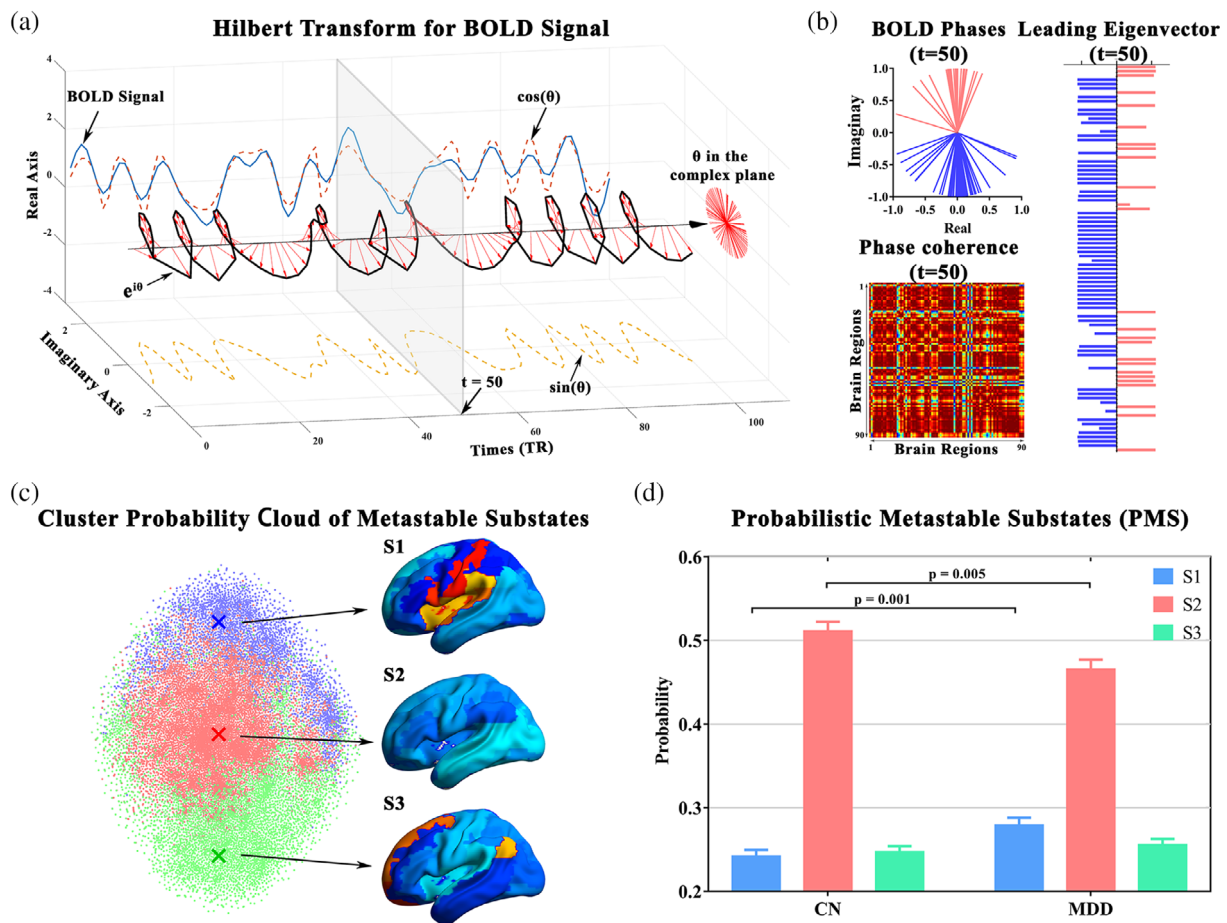
FIGURE 1 Computing the probabilistic metastable substate (PMS) space for whole-brain activity. (a) Leading eigenvector dynamics analysis (LEiDA) method for the time series in every brain region of each participant. (b) Blood-oxygenation-level-dependent (BOLD) phase coherence matrix and its leading eigenvector at a given time point. (c) Clustering analysis for leading eigenvectors at all time points in all subjects. Each cluster is represented by a central vector (green, red, and blue), representing a recurrent pattern of phase coherence or substate. (d) Three PMS spaces for major depressive disorder (MDD) and health. Substates 1 and 2 are significantly different in terms of the probability of occurrence between MDD and health.

dimensionality of the coherence matrix, which can capture the instantaneous dominant connectivity pattern for each time point. Next, based on the leading eigenvector of the phase coherence matrix for each time point, the PMS space was defined by the k cluster centroids, which were obtained from the time-resolved leading eigenvectors across the time points and subjects using k-means clustering algorithm (Figure 1c). Notably, the number of PMSs present is a free parameter and the optimal number of clusters in our study was $k = 3$ according to the Silhouette index and the minimal p value for significant differences between probabilities between MDD patients and healthy controls.

Finally, following the identification of metastable substates, the probability of occurrence of each FC state was computed for all subjects. The probability of occurrence or fractional occupancy is simply the ratio of the number of epochs assigned to a given cluster centroid divided by the total number of epochs (TRs) in each group. Differences in probabilities of occurrence were statistically assessed between MDD patients and healthy controls using a two-tailed two-sample t-test with a significance threshold of $p = .05$ and Bonferroni correction.

2.5 | Whole-brain computational model construction and optimization

2.5.1 | Whole-brain DFM model construction

Based on the characteristics of the brain states using the leading eigenvector dynamics analysis (LEiDA) method, we propose a computational framework for the large-scale whole-brain model to generate such brain states to promote or force the transition between states. Briefly, we adopted the biophysics-based large-scale computational model proposed by Deco et al. (Deco, Ponce-Alvarez, et al., 2014; Kringelbach et al., 2020), which reduces the complexity and number of local microcircuit parameters in a spiking neural network model using a dynamical mean-field (DMF) approach. Specifically, the DMF model uses a reduced set of dynamical equations describing the activity of coupled excitatory and inhibitory neuron pools to describe the activity of large ensembles of interconnected excitatory and inhibitory spiking neurons. The inhibitory currents are mediated by γ-aminobutyric acid (GABA) type A receptors, whereas excitatory
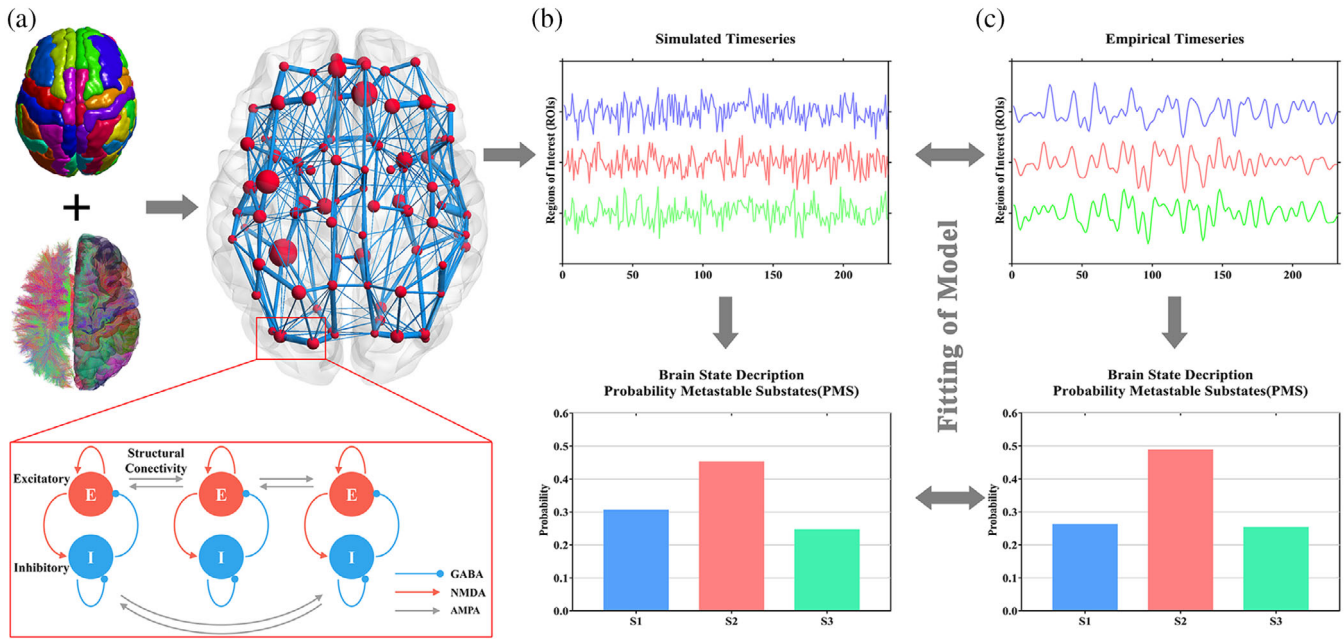
FIGURE 2 Schematic of the whole-brain computational model. (a) the whole-brain model with the local dynamic mean-field model, in which then underlying anatomical connectivity was determined using diffusion MRI and tractography techniques. (b) Simulated time series and its corresponding simulated probabilistic metastable substate (PMS) space. (c) Empirical time series from the empirical functional magnetic resonance imaging (fMRI) and its corresponding empirical PMS space. Notably, the whole-brain model was fitted to the empirical neuroimaging data described by the PMS space.

synaptic currents are mediated by N-methyl-D-aspartate (NMDA) receptors. Importantly, in the large-scale computational model, each brain region receives excitatory input from all structurally connected regions into its excitatory pool, weighted by the underlying anatomical connectivity matrix obtained from DTI (Figure 2a). Notably, emulating the resting-state condition, we used parameters in the DMF model based on the findings of Wong and Wang (Wong & Wang, 2006) such that each isolated node exhibited typical noisy spontaneous activity with a low firing rate ($r^{(E)} \sim 3\,Hz$) observed in electrophysiology experiments. Finally, the generalized hemodynamic model was used to transform the simulated mean-field activity from the whole-brain DMF model into a BOLD signal. In our study, we used all biophysical parameters stated by Stephan et al. (Stephan et al., 2007) and concentrated on the most functionally relevant frequency range for resting-state activity, that is, both simulated and empirical, and BOLD signals were band-pass filtered between 0.01 and 0.08 Hz.

2.6 | Empirical fitting of the whole-brain model

2.6.1 | Comparing empirical and simulated PMS space measurements

By running the large-scale whole-brain computational model, the simulated BOLD signals and corresponding probabilities of the metastable substates were assessed. Specifically, the leading eigenvector of each simulated time point was classified according to the Euclidean distance from the extracted empirical centers after clustering. The probabilities of the metastable substates from the simulated signals were calculated as the ratio of the number of epochs assigned to a given empirical cluster centroid (Figure 2b). Then, a symmetrized Kullback–Leibler (KL) distance was considered to compare the empirical and simulated probability metastable space state measurements (Figure 2c), as follows:

$$KL(P_{emp}, P_{sim}) = 0.5\left(\sum_i P_{emp}(i)\ln\left(\frac{P_{emp}(i)}{P_{sim}(i)}\right) + \sum_i P_{sim}(i)\ln\left(\frac{P_{sim}(i)}{P_{emp}(i)}\right)\right)$$

(2)

where $P_{emp}(i)$ and $P_{sim}(i)$ are the empirical and simulated probabilities of the same empirically extracted metastable substates i, respectively.

2.6.2 | Empirical fitting of global coupling factor across all subjects

The global coupling factor (G) is a free control parameter that is varied systematically to study the dynamics of the global cortical system that equally scales all interarea E-to-E connections. Finding the optimal working point of the system requires the optimal G value such that the simulated activity by the model maximally fits the empirical resting-state activity of all participants. Therefore, the averaged structural connectivity across all subjects (including MDD patients and healthy controls) was calculated and considered as the underlying

anatomical connectivity matrix. Then, the whole-brain computational model for all subjects was run 10 times with a time step of 1 ms for a range of G values between 0.5 and 5 (with increments of 0.1). The 2000s simulated BOLD signals were obtained for each G value and were down-sampled into 1000 time points according to 2 s of the empirical BOLD signals. Finally, the KL distance was calculated between the simulated and empirical corresponding probabilities of the metastable substates for each G value.

2.6.3 | Empirical fitting of structural connectivity for the specific models

Based on the optimal G value, the special whole-brain models of MDD and health were optimized to characterize the specific brain activity and the metastable substates. In both cases, two group-averaged structural connectomes were calculated for MDD patients and healthy controls and were considered as the underlying anatomical connectivity matrix. Then, the underlying anatomical connectivity matrix is optimized by computing the distance between the model $FC_{ij}^{\text{phase-mod}}$ and empirical grand-averaged phase coherence matrices using a gradient-descent approach. The model was run repeatedly with the optimized anatomical connectomes until the fit converged toward a stable value. The anatomical connectomes were updated using the following procedure:

$$C_{ij} = C_{ij} + \varepsilon \left(FC_{ij}^{\text{phase-emp}} - FC_{ij}^{\text{phase-mod}} \right) \quad (3)$$

where $\varepsilon = 0.01$, and the grand-averaged phase coherence matrix is defined as follows:

$$FC_{ij} = \left\langle \cos \left(\theta_j(t) - \theta_i(t) \right) \right\rangle \quad (4)$$

where $\theta_j(t)$ is the phase of the BOLD signal in brain regions j at time t extracted with the Hilbert transform, and the bracket denotes the average over time.

2.7 | Forcing brain states transitions between MDD and health

Based on two fitted specific whole-brain computational models for MDD and health, our study further explores how to force the transition of brain metastable substates between MDD patients and healthy subjects. To address this challenge, excitatory or inhibitory external stimulations were added to the fitted whole-brain computational model to probe the alteration of brain metastable substates. A previous study suggested that the whole-brain model can simulate task-evoked activity through external stimulation (Deco, Ponce-Alvarez, et al., 2014). Therefore, each brain region was systematically perturbed in the whole-brain model through an excitatory or inhibitory stimulation intensity of 0.02 in our study. Particularly, in the

fitted whole-brain model for MDD, only one brain area is stimulated at a time, and the excitatory stimulation intensity is 0.02.

For each external excitatory stimulation, we calculated the KL distance between the model-based PMSs of the whole-brain model for MDD patients and the empirical PMSs of healthy controls. Correspondingly, we perturbed only one region of the healthy whole-brain model at a time through an inhibitory stimulation intensity of −0.02 and calculated the KL distance with the empirical PMSs of MDD patients. In addition, we further probed the effects of different intensities of stimulation on forcing transitions of brain states between MDD and healthy subjects. The intensity of excitatory or inhibitory stimulation was set to 0.01, 0.05, and 0.08.

3 | RESULTS

3.1 | PMS space for whole-brain activity

To accurately probe the stimulus-driven transition of brain states between MDD patients and healthy controls, we first provide a quantitative characterization of the dynamics of underlying brain states. The PMS space for the human brain of MDD and the health was assessed using LEiDA method (Deco et al., 2017; Deco et al., 2019; Kringelbach et al., 2020). Our results showed that, as expected, MDD patients and healthy controls could be significantly distinguished by the three substates based on LEiDA methods (Figure 1d), demonstrating that the clustering approach is useful for distinguishing brain states. Specifically, compared to healthy controls, the probability of substate 1 (S1) was significantly increased in MDD patients ($t = -3.19$, $p = .0016$; two-sample t-test with Bonferroni correction). In contrast, the probability of substate 2 (S2) was significantly decreased ($t = 2.81$, $p = .0054$; two-sample t-test with Bonferroni correction).

3.2 | The optimal spatiotemporal fit of the whole-brain model to the PMS space

Based on the characteristics of the brain states using the LEiDA method, we built the large-scale whole-brain model with DFM to generate such brain states to promote or force the transition between states. Noteworthy, we adopted the two-step strategy of fitting the whole-brain model to the PMS space for MDD patients and healthy subjects through optimizing the global coupling parameters and structural connectivity between brain areas. Based on the structural connectivity averaged across all subjects, we first fitted the whole-brain model to the PMS space of all subjects by exhaustively exploring the global coupling parameter (G) across a range of 0.5–5 (with increments of 0.1). Our results show that the different G values yield significantly different KL distances between the empirical and modeled PMSs (Figure 3a). The minimum KL distance was 0.0064, corresponding to a G value of 2.6, suggesting the optimal fitting of the spatiotemporal characteristics.
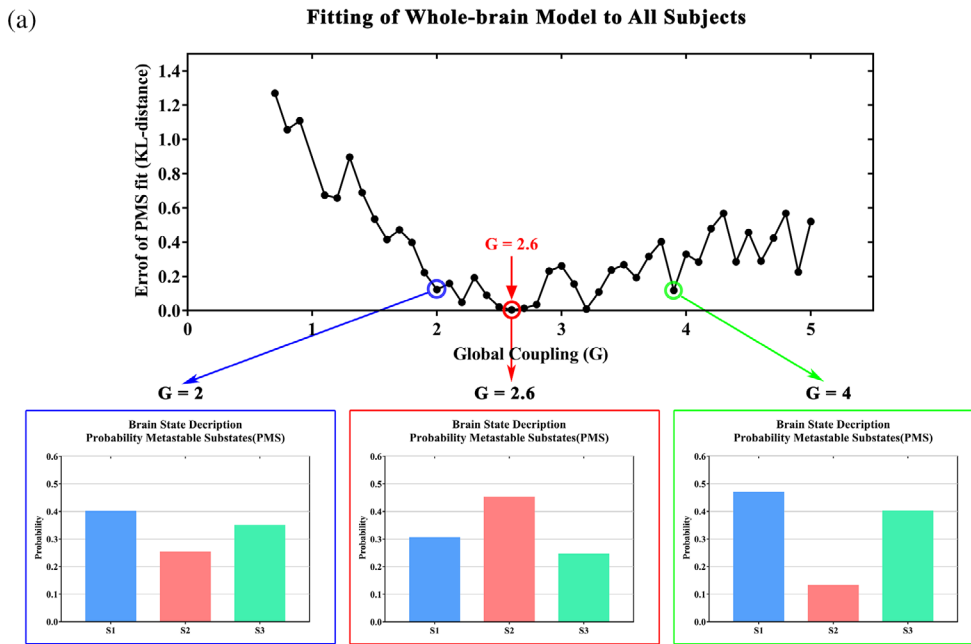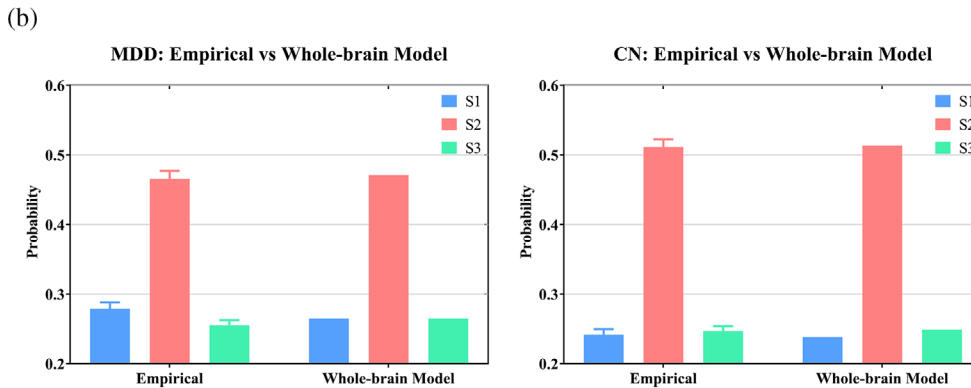
(a)

(b)

Upon optimal global coupling (G = 2.6), we further optimized the whole-brain computational models for radically different brain states of MDD patients and healthy controls. Based on the structural connectivity averaged across each group, we measured respectively the difference between the model and the empirical group-average phase coherence matrices for MDD and the health and then adjusted the structural connections separately using a gradient-descent approach. The whole-brain model was run repeatedly with recursive updates of the structural connectivity until convergence was reached. We continued adopting the KL distance during optimization to evaluate the similarity between the modeled and empirical PMSs. Our results showed that we successfully used the whole-brain models to fit the PMS space of brain states in MDD patients and healthy controls (Figure 3b). Specifically, the KL distance between the empirical MDD PMS space and the modeled PMS space obtained by the best-fit model for MDD was 2.20×10^{-4}. The probabilities of the three substates from the modeled BOLD time series were 0.2698 (S1), 0.4709 (S2), and 0.2593 (S3), and the corresponding probabilities of the three substates from the empirical BOLD data of MDD were 0.2792 ± 0.0981 (S1), 0.4653 ± 0.1312 (S2), and 0.2555 ± 0.1312 (S3).

Similarly, the KL distance between the empirical PMS space of the healthy controls and the modeled PMS space obtained by the best-fit model for the healthy controls was 3.99×10^{-5}. The probabilities of the three substates from the modeled BOLD time series were 0.2881 (S1), 0.5132 (S2), and 0.24876 (S3), and the corresponding probabilities of the three substates from the empirical MDD BOLD data were 0.2419 ± 0.0083 (S1), 0.5110 ± 0.1224 (S2), and 0.2471 ± 0.0765(S3).

3.3 | Forcing brain state transitions between MDD patients and healthy controls

Our results showed that we could successfully create whole-brain models that fit the empirical fMRI data from MDD patients and healthy controls. However, the primary purpose of our study was to attempt to address the fundamental question of how to drive the brain's transition between health and depressive disorders through external stimulation, which is extremely important for the translation to clinical contexts and demonstrable clinical utility. The whole-brain computational model with DMF provided an effective way of
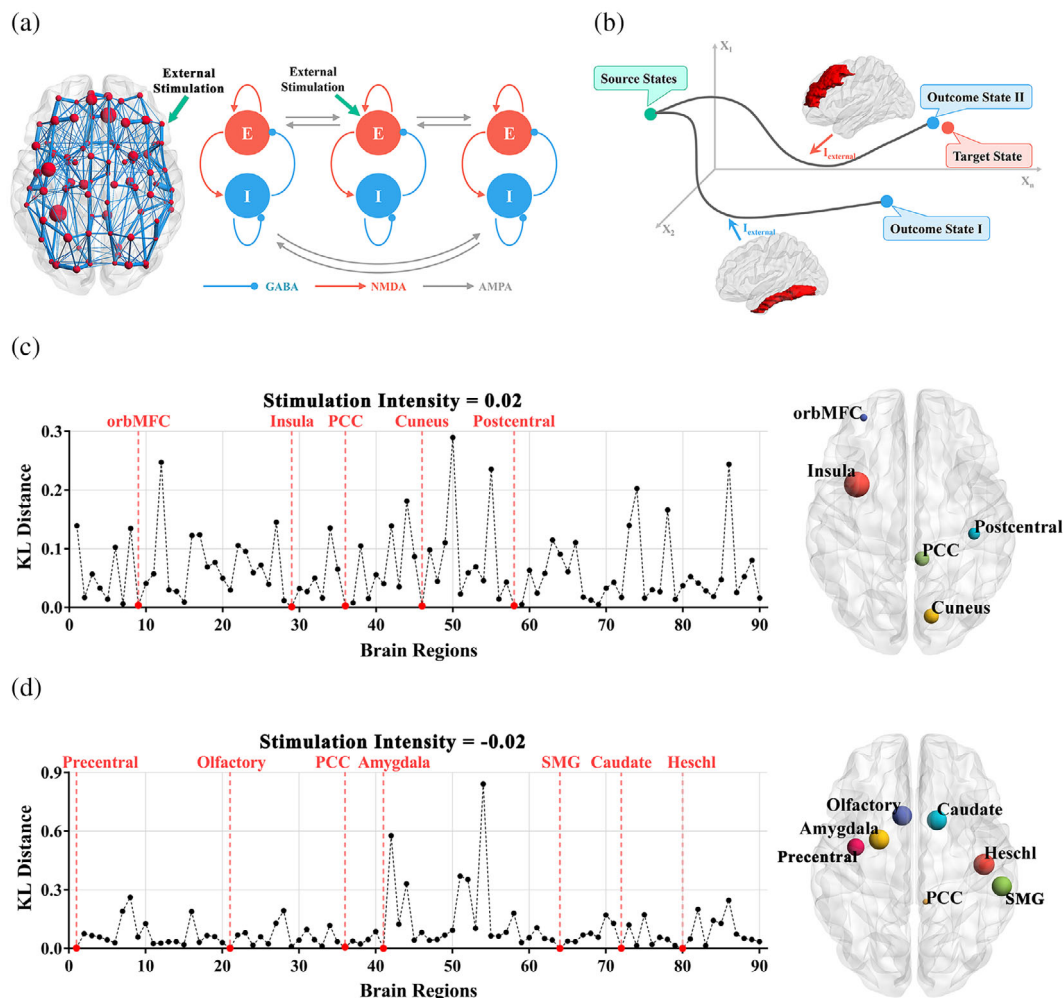
FIGURE 4 Forcing the transition of brain states between major depressive disorder (MDD) and heath. (a) The whole-brain model with external excitatory or inhibitory stimulation. (b) Schematic of the strategy for forcing the transition between source and target brain states. (c) Forcing the transition from MDD to health by excitatory external stimulation (intensity = 0.02). (d) Forcing the transition from health to MDD by external inhibitory stimulation (intensity = 0.02)

perturbing the substates of the brain by simply adding external excitatory or inhibitory stimulation to the excitatory neuron population (Figure 4a). In our study, each brain region in the fitted whole-brain model was systematically stimulated by an excitatory or inhibitory stimulation. Then, we compared the resulting model-based PMS space with the empirical data for the other target states. In particular, we added excitatory stimulation (intensity = 0.02) to each brain region in the fitted MDD model and then compared the modeled PMS distribution with the empirical PMS distribution from healthy controls. Our results showed that forcing the transition of brain states from MDD patients to healthy controls can be achieved by exciting the brain activity of the insula (KL with the empirical PMS space from healthy controls = 8.57×10^{-4}), cuneus (KL = 2.5×10^{-3}), posterior cingulate cortex (PCC; KL = 2.5×10^{-3}), postcentral gyrus (KL = 2.9×10^{-3}), and orbitofrontal gyrus (KL = 3.6×10^{-3}; Figure 4b). Correspondingly, we also added the inhibitory stimulation (intensity = -0.02) to each brain region in the fitted model for the healthy and found that forcing the transition of the brain from health

to MDD can be achieved by inhibiting the activity of PCC (KL of the empirical MDD PMS space = 7.4×10^{-3}), amygdala (KL = 1.3×10^{-3}), caudate (KL = 1.5×10^{-3}), precentral gyrus (KL = 2.6×10^{-3}), olfactory cortex (KL = 1.6×10^{-3}), supramarginal gyrus (KL = 1.4×10^{-3}), and Heschel gyrus (KL = 1.0×10^{-3}; Figure 4c). We also examined the effect of different external stimulation intensities (intensity = 0.01, 0.05, and 0.08) on forcing transitions of brain states between MDD patients and healthy controls. Our results showed that the brain regions that forced the transition of brain states varied at different intensities of external stimulation. At excitatory stimulation with small intensity (intensity = 0.01), the transition of brain states from MDD to healthy was mainly achieved by the precentral gyrus, dorsolateral superior frontal gyrus, precuneus, middle cingulate cortex, and angular gyrus. And the transition of brain states was mainly achieved via the postcentral gyrus, inferior parietal gyrus, PCC, putamen, and hippocampus under medium stimulation (intensity = 0.05) and by the middle frontal gyrus and the inferior occipital gyrus at high excitatory stimulation (intensity = 0.08;
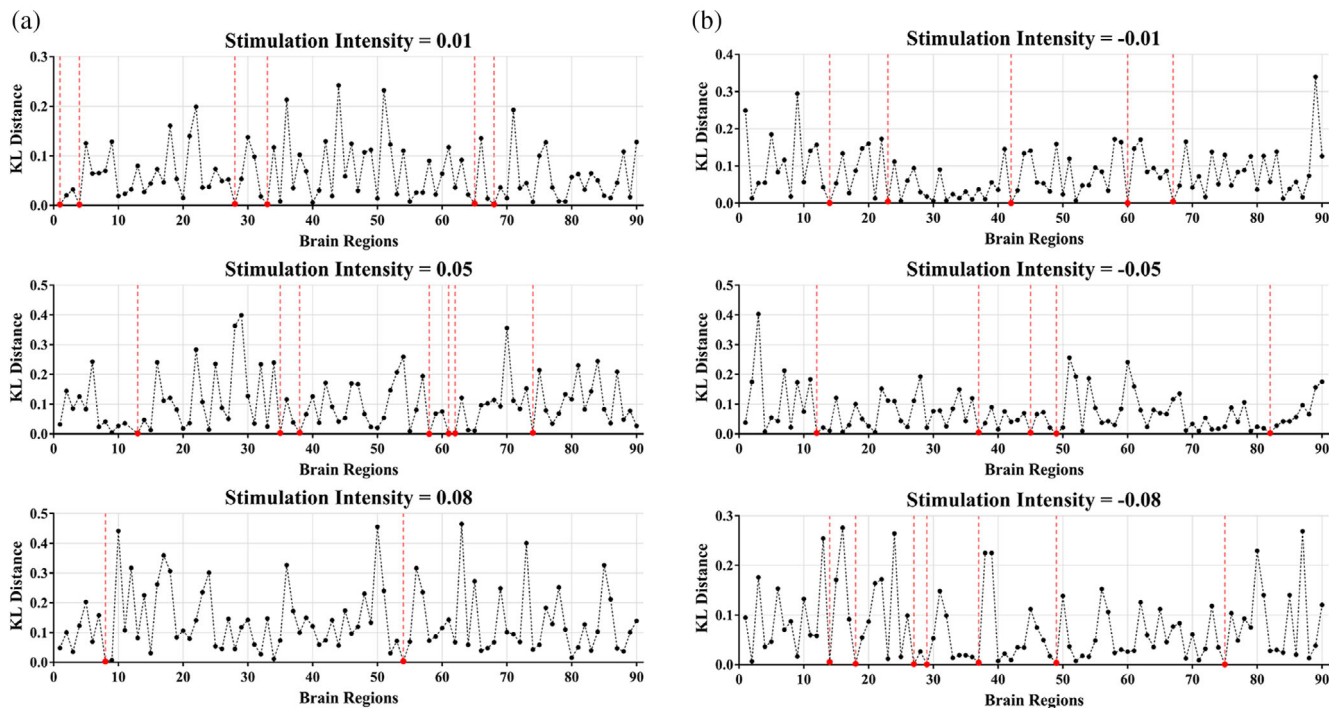
FIGURE 5 Impact of different external stimulation intensities on the transition between major depressive disorder (MDD) and health and vice versa. (a) Forcing transitions from MDD to health by excitatory stimulation with different intensities. (b) Forcing transitions from health to MDD by inhibitory stimulation with different intensities

Figure 5a). Similarly, the transition of brain states from health to MDD was mainly achieved via the amygdala, superior parietal gyrus, precuneus, and the orbital medial frontal gyrus under low inhibitory stimulation (intensity = −0.01), via the superior occipital, temporal gyrus, cuneus, and hippocampus under medium inhibitory stimulation (intensity = −0.05), and via the insula, pallidum, hippocampus, rectus gyrus, and superior occipital under high inhibitory stimulation (intensity = −0.08; Figure 5b).

4 | DISCUSSION

In this study, we constructed a biophysically based large-scale dynamic model of human brain activity that fits the PMS spaces of the unequal brain states of participants with MDD and healthy controls. Then, we explored the forced transition between different brain states from MDD and health via excitatory or inhibitory stimulation. In particular, we implemented a large-scale dynamical system at the whole-brain level, using a balanced DMF model, and optimized the whole-brain dynamic model to fit the respective PMS space of MDD patients and healthy controls. Through excitatory or inhibitory external stimulation of the whole-brain dynamical model, we successfully predicted the optimal brain regions to promote the transition of brain states between MDD and health. Collectively, our findings suggest that we can build large-scale whole-brain models to characterize all brain states for depression and health and potentially optimize the external stimulation strategy by changing the cloud of metastable substates from that found in depression to health.

Brain state definition in systems neuroscience has justifiably drawn and continues to draw a great deal of attention. Early attempts have been made to define brain states in various ways and focused on brain states in a state space, a high-dimensional coordinate system characterizing the brain's activity at a given time. Lastly, some approaches have proposed describing a brain state as an attractor of interacting brain regions but have failed to capture all aspects of the rich functional dynamics of brain states (Deco & Jirsa, 2012; Gu et al., 2018; Shanahan, 2010; Tognoli & Kelso, 2014). Our study adopted a novel framework called LEiDA to characterize PMSs as a stochastic subdivision of regular and persistent brain states (Cabral et al., 2017; Deco et al., 2019). This approach uses the BOLD phase signal to determine the state of whole-brain synchronization between different brain regions across various time points (Deco et al., 2017). This was computed for all participants, and group results were clustered to find the metastable substates where their probability of occurrence characterizes a given brain state. The LEiDA framework is highly flexible, robust, and precise and can detect and characterize recurrent substates for resting states or tasks in the healthy brain (Cabral et al., 2017; Stark et al., 2019). It can also distinguish between brain states in disease (Figueroa et al., 2019) and even in altered states, such as the effects of psilocybin (Kringelbach et al., 2020; Lord et al., 2019) and sleep (Deco et al., 2019). Therefore, we adopted the LEiDA framework to detect the metastable substates from resting-state fMRI for MDD patients and healthy controls and found a significant alteration in the characterization of MDD substates. Notably, our results from the whole-brain model fitting also showed that the

simulated PMS space could describe the necessary and sufficient dynamic features of the functional empirical data, consistent with the previous study.

Whole-brain models aim to balance complexity and realism to describe the most important functional features of the brain in vivo (Breakspear et al., 2010; Deco et al., 2010). The fundamental principle links anatomical structures with functional dynamics (Deco et al., 2009; Jirsa et al., 2002). The anatomy can be represented in many ways, ideally through large-scale tract-tracing providing directional anatomical connectivity, which can be obtained using diffusion MRI combined with probabilistic tractography (Basser & Pierpaoli, 1996; Hagmann et al., 2010; Markov et al., 2013). Functional global dynamics emerge from the mutual interactions of local node dynamics coupled with the underlying empirical anatomical connectivity. Local neuronal dynamics can be expressed as a spiking neuronal network (Deco & Jirsa, 2012), mean-field model (Deco & Kringelbach, 2014; Deco, McIntosh, et al., 2014; Honey et al., 2007), or mesoscopic model (Deco et al., 2018; Freyer et al., 2012). Then, these models fit the empirical data by optimizing the global coupling parameter that scales the underlying structural connectivity or adapting the effective connectivity that models potential heterogeneity in conductivity. Recent developments have shown that whole-brain models can provide insights into the underlying dynamics of the brain, including static FC and dynamic measurements. In addition, whole-brain models can be used to explain brain activity on faster timescales (ms) (Kringelbach & Deco, 2020). Therefore, based on the PMS captured by LEiDA, we constructed a large-scale whole-brain dynamical model based on the dynamical mean-field model and optimized the global coupling parameter to fit the PMS space from all empirical data. Then, we further optimized the whole-brain model by adapting the effective connectivity and successfully fitting the PMS space of the two radically different brain states of MDD and health.

The large-scale whole-brain model improves our understanding of human brain function. More importantly, it has enormous potential for studying stimulation-induced state transitions, derived from its powerful ability for exhaustive searching and optimizing all underlying parameters and locations. In particular, we can exhaustively stimulate offline a realistic whole-brain model that can accurately model different brain states. Then, we can detect the best strategy of stimulation that is most effective in forcing a transition from an initial state to the desired target state. A recent study validated this basic idea by constructing a whole-brain model that successfully fit the PMS space of the two radically different brain states of human sleep and wakefulness and investigated the best strategy of stimulation to force transitions between these states (Deco et al., 2019). In clinical practice, the desired transition would aim for a homeostatic rebalancing of healthy whole-brain dynamics from inordinate whole-brain dynamics to predict the best strategy for recovery. Based on these basic ideas, we stimulated the optimized whole-brain model by adding excitatory or inhibitory external stimulation to each brain region to detect the most efficient stimulation loci to force the transition of brain states between MDD and health.

Determination of the optimal method of controlling the brain and its transition from depression to health still involves many unknown challenges. However, our study provides the first evidence for the externally controlled transitions of brain states between MDD and health utilizing stimulation of the whole-brain model. We found that the transition from MDD to health could be achieved by enhancing the excitation of local microcircuits in the insula, cuneus, PCC, medial orbitofrontal cortex, and postcentral gyrus. The insula is a critical brain structure for integrating affective and cognitive memory, saliency processing, and attention switching (Chiarello et al., 2013; Uddin et al., 2017; Wang, Wei, et al., 2020). Numerous evidence has shown that structural and functional abnormalities in the insula are widely observed in patients with MDD. Meanwhile, an increasing number of MRI studies have also found that structural and functional abnormalities in the insula can be normalized after optimizing treatments, including modified electroconvulsive therapy (mECT) (Dichter et al., 2015; Moon et al., 2021; Wang, Wei, et al., 2020), transcranial magnetic stimulation (Fu et al., 2021), transcranial direct current stimulation (Sagliano et al., 2019; Sankarasubramanian et al., 2017). For example, a recent study found that pretreatment decreased FC with the insula and normalization of this area's function after mECT (Wang, Wei, et al., 2020). In addition, the PCC is a key region of the DMN with strong connectivity with the entorhinal cortex in primates. The PCC is consistently engaged in a range of tasks that examine episodic memory, including autobiographical memory, the imagination of the future, spatial navigation, and scene processing (Vann et al., 2009). It has also been shown that the PCC's FC is related to rumination in depression and the antidepressant effects of mECT and other treatments, such as deep brain stimulation. In particular, a recent study found that voxels in the PCC had significantly increased FC with the orbitofrontal cortex; in participants receiving medication, FC between the lateral orbitofrontal cortex and PCC decreased back to that in the controls (Cheng, Rolls, Qiu, Xie, et al., 2018). The orbitofrontal cortex in primates, including humans, is the key brain area in emotion and in the representation of reward value and non-reward, which does not obtain an expected reward (Grabenhorst & Rolls, 2011; Rolls, 2014). Previous studies have also suggested that the orbitofrontal cortex is a key target to ameliorate depression (Rolls, 2016, 2017). Meanwhile, some aspects of depression may be related to over-responsiveness of the lateral orbitofrontal cortex to nonreward and punishment conditions, and under-responsiveness of the medial orbitofrontal cortex could contribute to other aspects of depression such as anhedonia. Consistent with these results above, our findings show that the insula, PCC, and orbitofrontal cortex play important roles in the neuropathology of MDD and antidepressant treatment.

Furthermore, we also found that the transition from MDD to health could be achieved by enhancing the inhibition of local microcircuits in the PCC, amygdala, olfactory cortex, caudate, precentral gyrus, Heschel gyrus, and supramarginal gyrus. The amygdala, a pivotal component of the affective network, is a critical brain region for both bottom-up and top-down processes of emotion generation and regulation, highlighted in the pathology of MDD. The caudate, the main sub-region of the striatum, is a central locus for reward-based

behavioral learning and is therefore intricately involved in pleasure and motivation. Decreased connectivity and the amygdala and caudate have been reported to be strongly implicated in hopelessness and anhedonia, the debilitating symptoms of MDD (Ramasubbu et al., 2014). In addition, the olfactory system and emotion share many common structures, which provide a framework for bridging gaps between cognitive and olfactory function via a similar neuropathological basis of depression. A recent study showed that participants with MDD had mood dysregulation, coupled with significantly impaired response inhibition and olfactory functions (Wang, Jin, et al., 2020). Consistent with these findings, our study showed that inhibiting the activity of regions including the PCC, amygdala, olfactory cortex, and caudate can force the transition of brain states from health to MDD.

The whole-brain model provides a possible basis for the precise prediction of the effects of external perturbations needed to force transitions of brain states between MDD and health. However, the limitations of the current study should be considered. First, to reduce the complexity of modeling, the brain is typically divided into a meaningful parcellation based on structural and functional information. In our study, we used the AAL template to obtain the structural connectivity from DTI and BOLD time series from rs-fMRI. Previous studies have suggested that the AAL atlas is not encouraged in functional connectivity analysis (Sala-Llonch et al., 2019; Smith et al., 2011). However, the different parcellations maybe increase the spatial granularity, but they come with the cost of increasing the complexity of the model and decreasing its robustness of the model. Previous studies on the whole-brain model have suggested the brain can be divided into 80–150 ROIs to reduce the complexity of modeling (Eickhoff, Constable, & Yeo, 2018; Eickhoff, Yeo, & Genon, 2018; Kringelbach & Deco, 2020). Meanwhile, the AAL template also has relatively robust results on PMSs and the whole-brain model (Deco et al., 2019; Deco & Kringelbach, 2014; Figueroa et al., 2019; Kringelbach et al., 2020). Second, the white matter (WM) signal was regressed out to focus on the gray matter (GM) signals, which might be another limitation of our study. However, more and more evidence suggested brain white-matter (WM) signals obtain using BOLD-fMRI provide functional information about intrinsic activity and can be used to characterize its connectivity (Gong-Jun Ji et al., 2017; Li et al., 2019; Li et al., 2021). A recent study has identified and replicated robust decreased small-world topology in two completely independent samples of MDD. The small-world topology of the WM functional connectome may be the potential biomarker of MDD-related early prognosis and diagnosis (Li, Chen, et al., 2020). In addition, other studies also suggested that the WM function connectome is unlikely to be generated by noise and may provide important information to understand the underlying mechanisms of cognition and behavior (Li, Biswal, et al., 2020). Therefore, WM function connectomes might be contributed to the whole-brain model construction and optimization and further improve the robustness and generalization of the model.

Overall, our findings suggest that large-scale whole-brain imaging has great clinical potential by providing novel biophysical evidence for the neural mechanism of MDD and its recovery and opening possibilities for discovering novel stimulation targets for the treatment of MDD.

AUTHOR CONTRIBUTIONS

Conceptualization and Formal Analysis: Shengpei Wang and Hongwei Wen; Methodology, Software, and Visualization: Shengpei Wang and Shuang Qiu; Data Curation: Hongwei Wen and Peng Xie; Writing-Original draft and writing-Review & Editing: Shengpei Wang, Hongwei Wen, and Shuang Qiu; Supervision, Project Administration and Funding acquisition: Jiang Qiu and Huiguang He.

CONFLICT OF INTEREST

All authors declare no competing interests.

DATA AVAILABILITY STATEMENT

The datasets generated and/or analysed as well as code used during the current study are available from the corresponding author upon reasonable request.

ORCID

Jiang Qiu https://orcid.org/0000-0003-0269-5910
Huiguang He https://orcid.org/0000-0002-0684-1711

REFERENCES

Adhikari, M. H., Hacker, C. D., Siegel, J. S., Griffa, A., Hagmann, P., Deco, G., & Corbetta, M. (2017). Decreased integration and information capacity in stroke measured by whole brain models of resting state activity. *Brain: A Journal of Neurology*, *140*(4), 1068–1085. https://doi.org/10.1093/brain/awx021

Aerts, H., Schirner, M., Dhollander, T., Jeurissen, B., Achten, E., van Roost, D., Ritter, P., & Marinazzo, D. (2020). Modeling brain dynamics after tumor resection using the virtual brain. *NeuroImage*, *213*, 116738. https://doi.org/10.1016/j.neuroimage.2020.116738

Basser, P. J., & Pierpaoli, C. (1996). Microstructural and physiological features of tissues elucidated by quantitative-diffusion-tensor MRI. *Journal of Magnetic Resonance, Series B*, *111*(3), 209–219. https://doi.org/10.1006/jmrb.1996.0086

Bassett, D. S., & Bullmore, E. T. (2009). Human brain networks in health and disease. *Current Opinion in Neurology*, *22*(4), 340–347. https://doi.org/10.1097/WCO.0b013e32832d93dd

Bora, E., Fornito, A., Pantelis, C., & Yücel, M. (2012). Gray matter abnormalities in major depressive disorder: A meta-analysis of voxel based morphometry studies. *Journal of Affective Disorders*, *138*(1–2), 9–18. https://doi.org/10.1016/j.jad.2011.03.049

Brakowski, J., Spinelli, S., Dörig, N., Bosch, O. G., Manoliu, A., Holtforth, M. G., & Seifritz, E. (2017). Resting state brain network function in major depression – Depression symptomatology, antidepressant treatment effects, future research. *Journal of Psychiatric*

Research, *92*, 147–159. https://doi.org/10.1016/j.jpsychires.2017.04.007

Braun, U., Schaefer, A., Betzel, R. F., Tost, H., Meyer-Lindenberg, A., & Bassett, D. S. (2018). From maps to multi-dimensional network mechanisms of mental disorders. *Neuron*, *97*(1), 14–31. https://doi.org/10.1016/j.neuron.2017.11.007

Breakspear, M. (2004). "Dynamic" connectivity in neural systems. *Neuroinformatics*, *2*(2), 205–226. https://doi.org/10.1385/ni:2:2:205

Breakspear, M., Jirsa, V., & Deco, G. (2010). Computational models of the brain: From structure to function. *NeuroImage*, *52*(3), 727–730. https://doi.org/10.1016/j.neuroimage.2010.05.061

Bullmore, E., & Sporns, O. (2009). Complex brain networks: Graph theoretical analysis of structural and functional systems. *Nature Reviews Neuroscience*, *10*(3), 186–198. https://doi.org/10.1038/nrn2575

Cabral, J., Kringelbach, M. L., & Deco, G. (2017). Functional connectivity dynamically evolves on multiple time-scales over a static structural connectome: Models and mechanisms. *NeuroImage*, *160*, 84–96. https://doi.org/10.1016/j.neuroimage.2017.03.045

Cheng, W., Rolls, E. T., Qiu, J., Xie, X., Wei, D., Huang, C.-C., Yang, A. C., Tsai, S. J., Li, Q., Meng, J., Lin, C. P., Xie, P., & Feng, J. (2018). Increased functional connectivity of the posterior cingulate cortex with the lateral orbitofrontal cortex in depression. *Translational Psychiatry*, *8*(1), 1–10. https://doi.org/10.1038/s41398-018-0139-1

Cheng, W., Rolls, E. T., Qiu, J., Yang, D., Ruan, H., Wei, D., Zhao, L., Meng, J., Xie, P., & Feng, J. (2018). Functional connectivity of the precuneus in unmedicated patients with depression. *Biological Psychiatry. Cognitive Neuroscience and Neuroimaging*, *3*(12), 1040–1049. https://doi.org/10.1016/j.bpsc.2018.07.008

Chiarello, C., Vazquez, D., Felton, A., & Leonard, C. M. (2013). Structural asymmetry of anterior insula: Behavioral correlates and individual differences. *Brain and Language*, *126*(2), 109–122. https://doi.org/10.1016/j.bandl.2013.03.005

Dai, L., Zhou, H., Xiangyang, X., & Zuo, Z. (2019). Brain structural and functional changes in patients with major depressive disorder: A literature review. *PeerJ*, *7*, e8170. https://doi.org/10.7717/peerj.8170

Deco, G., Cruzat, J., Cabral, J., Knudsen, G. M., Carhart-Harris, R. L., Whybrow, P. C., Logothetis, N. K., & Kringelbach, M. L. (2018). Whole-brain multimodal neuroimaging model using serotonin receptor maps explains non-linear functional effects of LSD. *Current Biology*, *28*(19), 3065–3074.e6. https://doi.org/10.1016/j.cub.2018.07.083

Deco, G., Cruzat, J., Cabral, J., Tagliazucchi, E., Laufs, H., Logothetis, N. K., & Kringelbach, M. L. (2019). Awakening: Predicting external stimulation to force transitions between different brain states. *Proceedings of the National Academy of Sciences of the United States of America*, *116*(36), 18088–18097. https://doi.org/10.1073/pnas.1905534116

Deco, G., Jirsa, V., McIntosh, A. R., Sporns, O., & Kotter, R. (2009). Key role of coupling, delay, and noise in resting brain fluctuations. *Proceedings of the National Academy of Sciences*, *106*(25), 10302–10307. https://doi.org/10.1073/pnas.0901831106

Deco, G., & Jirsa, V. K. (2012). Ongoing cortical activity at rest: Criticality, multistability, and ghost attractors. *Journal of Neuroscience*, *32*(10), 3366–3375. https://doi.org/10.1523/jneurosci.2523-11.2012

Deco, G., Jirsa, V. K., & McIntosh, A. R. (2010). Emerging concepts for the dynamical organization of resting-state activity in the brain. *Nature Reviews Neuroscience*, *12*(1), 43–56. https://doi.org/10.1038/nrn2961

Deco, G., & Kringelbach, M. L. (2014). Great expectations: Using whole-brain computational connectomics for understanding neuropsychiatric disorders. *Neuron*, *84*(5), 892–905. https://doi.org/10.1016/j.neuron.2014.08.034

Deco, G., Kringelbach, M. L., Jirsa, V. K., & Ritter, P. (2017). The dynamics of resting fluctuations in the brain: Metastability and its dynamical cortical core. *Scientific Reports*, *7*(1), 3095. https://doi.org/10.1038/s41598-017-03073-5

Deco, G., McIntosh, A. R., Shen, K., Hutchison, R. M., Menon, R. S., Everling, S., Hagmann, P., & Jirsa, V. K. (2014). Identification of optimal structural connectivity using functional connectivity and neural modeling. *Journal of Neuroscience*, *34*(23), 7910–7916. https://doi.org/10.1523/jneurosci.4423-13.2014

Deco, G., Ponce-Alvarez, A., Hagmann, P., Romani, G. L., Mantini, D., & Corbetta, M. (2014). How local excitation-inhibition ratio impacts the whole brain dynamics. *The Journal of Neuroscience: The Official Journal of the Society for Neuroscience*, *34*(23), 7886–7898. https://doi.org/10.1523/JNEUROSCI.5068-13.2014

Delvecchio, G., Pigoni, A., Bauer, I. E., Soares, J. C., & Brambilla, P. (2020). Disease-discordant twin structural MRI studies on affective disorders. *Neuroscience and Biobehavioral Reviews*, *108*, 459–471. https://doi.org/10.1016/j.neubiorev.2019.11.023

Demirtaş, M., Burt, J. B., Helmer, M., Ji, J. L., Adkinson, B. D., Glasser, M. F., van Essen, D. C., Sotiropoulos, S. N., Anticevic, A., & Murray, J. D. (2019). Hierarchical heterogeneity across human cortex shapes large-scale neural dynamics. *Neuron*, *101*(6), 1181–1194.e13. https://doi.org/10.1016/j.neuron.2019.01.017

den Heuvel, V., Martijn, P., & Hulshoff Pol, H. E. (2010). Exploring the brain network: A review on resting-state fMRI functional connectivity. *European Neuropsychopharmacology*, *20*(8), 519–534. https://doi.org/10.1016/j.euroneuro.2010.03.008

den Heuvel, V., Martijn, P., & Sporns, O. (2013). Network hubs in the human brain. *Trends in Cognitive Sciences*, *17*(12), 683–696. https://doi.org/10.1016/j.tics.2013.09.012

Dichter, G. S., Gibbs, D., & Smoski, M. J. (2015). A systematic review of relations between resting-state functional-MRI and treatment response in major depressive disorder. *Journal of Affective Disorders*, *172*, 8–17. https://doi.org/10.1016/j.jad.2014.09.028

Dunlop, K., Talishinsky, A., & Liston, C. (2019). Intrinsic brain network biomarkers of antidepressant response: A review. *Current Psychiatry Reports*, *21*(9), 87. https://doi.org/10.1007/s11920-019-1072-6

Eickhoff, S. B., Constable, R. T., & Yeo, B. T. (2018). Topographic organization of the cerebral cortex and brain cartography. *NeuroImage*, *170*, 332–347. https://doi.org/10.1016/j.neuroimage.2017.02.018

Eickhoff, S. B., Yeo, B. T. T., & Genon, S. (2018). Imaging-based parcellations of the human brain. *Nature Reviews Neuroscience*, *19*(11), 672–686. https://doi.org/10.1038/s41583-018-0071-7

Figueroa, C. A., Cabral, J., Mocking, R. J. T., Rapuano, K. M., Hartevelt, T. J., Deco, G., Expert, P., Schene, A. H., Kringelbach, M. L., & Ruhé, H. G. (2019). Altered ability to access a clinically relevant control network in patients remitted from major depressive disorder. *Human Brain Mapping*, *40*(9), 2771–2786. https://doi.org/10.1002/hbm.24559

Fornito, A., & Bullmore, E. T. (2015). Connectomics: A new paradigm for understanding brain disease. *European Neuropsychopharmacology: The Journal of the European College of Neuropsychopharmacology*, *25*(5), 733–748. https://doi.org/10.1016/j.euroneuro.2014.02.011

Freyer, F., Roberts, J. A., Ritter, P., & Breakspear, M. (2012). A canonical model of multistability and scale-invariance in biological systems. *PLoS Computational Biology*, *8*(8), e1002634. https://doi.org/10.1371/journal.pcbi.1002634

Fu, Y., Long, Z., Luo, Q., Xu, Z., Xiang, Y., Du, W., Cao, Y., Cheng, X., & Du, L. (2021). Functional and structural connectivity between the left dorsolateral prefrontal cortex and insula could predict the antidepressant effects of repetitive transcranial magnetic stimulation. *Frontiers in Neuroscience*, *15*, 645936. https://doi.org/10.3389/fnins.2021.645936

Ghosh, A., Rho, Y., McIntosh, A. R., Kötter, R., & Jirsa, V. K. (2008). Cortical network dynamics with time delays reveals functional connectivity in the resting brain. *Cognitive Neurodynamics*, *2*(2), 115–120. https://doi.org/10.1007/s11571-008-9044-2

Gilson, M., Zamora-López, G., Pallarés, V., Adhikari, M. H., Senden, M., Campo, A. T., Mantini, D., Corbetta, M., Deco, G., & Insabato, A. (2020). Model-based whole-brain effective connectivity to study

distributed cognition in health and disease. *Network Neuroscience*, 4(2), 338–373. https://doi.org/10.1162/netn_a_00117

Gong-Jun Ji, W., Liao, F. C., Zhang, L., & Wang, K. (2017). Low-frequency blood oxygen level-dependent fluctuations in the brain white matter: more than just noise. Undefined. Retrieved from https://www.semanticscholar.org/paper/Low-frequency-blood-oxygen-level-dependent-in-the-Ji-Liao/d5d4ae550760c824a25a18238db8d8926df1198f

Grabenhorst, F., & Rolls, E. T. (2011). Value, pleasure and choice in the ventral prefrontal cortex. *Trends in Cognitive Sciences*, 15(2), 56–67. https://doi.org/10.1016/j.tics.2010.12.004

Gu, S., Cieslak, M., Baird, B., Muldoon, S. F., Grafton, S. T., Pasqualetti, F., & Bassett, D. S. (2018). The energy landscape of neurophysiological activity implicit in brain network structure. *Scientific Reports*, 8(1), 2507. https://doi.org/10.1038/s41598-018-20123-8

Hagmann, P., Cammoun, L., Gigandet, X., Gerhard, S., Ellen Grant, P., Wedeen, V., Meuli, R., Thiran, J. P., Honey, C. J., & Sporns, O. (2010). MR connectomics: Principles and challenges. *Journal of Neuroscience Methods*, 194(1), 34–45. https://doi.org/10.1016/j.jneumeth.2010.01.014

Hashemi, M., Vattikonda, A. N., Sip, V., Guye, M., Bartolomei, F., Woodman, M. M., & Jirsa, V. K. (2020). The Bayesian virtual epileptic patient: A probabilistic framework designed to infer the spatial map of epileptogenicity in a personalized large-scale brain model of epilepsy spread. *NeuroImage*, 217, 116839. https://doi.org/10.1016/j.neuroimage.2020.116839

Hock, R. S., Or, F., Kolappa, K., Burkey, M. D., Surkan, P. J., & Eaton, W. W. (2012). A new resolution for global mental health. *The Lancet*, 379(9824), 1367–1368. https://doi.org/10.1016/S0140-6736(12)60243-8

Honey, C. J., Kotter, R., Breakspear, M., & Sporns, O. (2007). Network structure of cerebral cortex shapes functional connectivity on multiple time scales. *Proceedings of the National Academy of Sciences*, 104(24), 10240–10245. https://doi.org/10.1073/pnas.0701519104

Jirsa, V. K., Jantzen, K. J., Fuchs, A., & Kelso, J. A. S. (2002). Spatiotemporal forward solution of the EEG and MEG using network modeling. *IEEE Transactions on Medical Imaging*, 21(5), 493–504. https://doi.org/10.1109/tmi.2002.1009385

Kerestes, R., Davey, C. G., Stephanou, K., Whittle, S., & Harrison, B. J. (2014). Functional brain imaging studies of youth depression: A systematic review. *NeuroImage: Clinical*, 4, 209–231. https://doi.org/10.1016/j.nicl.2013.11.009

Kringelbach, M. L., Cruzat, J., Cabral, J., Knudsen, G. M., Carhart-Harris, R., Whybrow, P. C., Logothetis, N. K., & Deco, G. (2020). Dynamic coupling of whole-brain neuronal and neurotransmitter systems. *Proceedings of the National Academy of Sciences of the United States of America*, 117(17), 9566–9576. https://doi.org/10.1073/pnas.1921475117

Kringelbach, M. L., & Deco, G. (2020). Brain states and transitions: Insights from computational neuroscience. *Cell Reports*, 32(10), 108128. https://doi.org/10.1016/j.celrep.2020.108128

Li, J., Biswal, B. B., Meng, Y., Yang, S., Duan, X., Cui, Q., Chen, H., & Liao, W. (2020). A neuromarker of individual general fluid intelligence from the white-matter functional connectome. *Translational Psychiatry*, 10(1), 1–12. https://doi.org/10.1038/s41398-020-0829-3

Li, J., Chen, H., Fan, F., Qiu, J., du, L., Xiao, J., Duan, X., Chen, H., & Liao, W. (2020). White-matter functional topology: A neuromarker for classification and prediction in unmedicated depression. *Translational Psychiatry*, 10(1), 1–10. https://doi.org/10.1038/s41398-020-01053-4

Li, J., Wu, G.-R., Li, B., Fan, F., Zhao, X., Meng, Y., Zhong, P., Yang, S., Biswal, B. B., Chen, H., & Liao, W. (2021). Transcriptomic and macroscopic architectures of intersubject functional variability in human brain white-matter. *Communications Biology*, 4(1), 1–14. https://doi.org/10.1038/s42003-021-02952-y

Li, J., Biswal, B. B., Wang, P., Duan, X., Cui, Q., Chen, H., & Liao, W. (2019). Exploring the functional connectome in white matter. *Human Brain Mapping*, 40(15), 4331–4344. https://doi.org/10.1002/hbm.24705

Lord, L.-D., Expert, P., Atasoy, S., Roseman, L., Rapuano, K., Lambiotte, R., Nutt, D. J., Deco, G., Carhart-Harris, R. L., Kringelbach, M. L., & Cabral, J. (2019). Dynamical exploration of the repertoire of brain networks at rest is modulated by psilocybin. *NeuroImage*, 199, 127–142. https://doi.org/10.1016/j.neuroimage.2019.05.060

Ma, K., Yu, J., Shao, W., Xu, X., Zhang, Z., & Zhang, D. (2020). Functional overlaps exist in neurological and psychiatric disorders: A proof from brain network analysis. *Neuroscience*, 425, 39–48. https://doi.org/10.1016/j.neuroscience.2019.11.018

Markov, N. T., Vezoli, J., Chameau, P., Falchier, A., Quilodran, R., Huissoud, C., Lamy, C., Misery, P., Giroud, P., Ullman, S., Barone, P., Dehay, C., Knoblauch, K., & Kennedy, H. (2013). Anatomy of hierarchy: Feedforward and feedback pathways in macaque visual cortex. *Journal of Comparative Neurology*, 522(1), 225–259. https://doi.org/10.1002/cne.23458

Medaglia, J. D., Lynall, M.-E., & Bassett, D. S. (2015). Cognitive network neuroscience. *Journal of Cognitive Neuroscience*, 27(8), 1471–1491. https://doi.org/10.1162/jocn_a_00810

Moon, S.-Y., Kim, M., Lho, S. K., Oh, S., Kim, S. H., & Kwon, J. S. (2021). Systematic review of the neural effect of electroconvulsive therapy in patients with schizophrenia: Hippocampus and insula as the key regions of modulation. *Psychiatry Investigation*, 18(6), 486–499. https://doi.org/10.30773/pi.2020.0438

Nixon, N. L., Liddle, P. F., Nixon, E., Worwood, G., Liotti, M., & Palaniyappan, L. (2014). Biological vulnerability to depression: Linked structural and functional brain network findings. *British Journal of Psychiatry*, 204(4), 283–289. https://doi.org/10.1192/bjp.bp.113.129965

Petersen, S. E., & Sporns, O. (2015). Brain networks and cognitive architectures. *Neuron*, 88(1), 207–219. https://doi.org/10.1016/j.neuron.2015.09.027

Ramasubbu, R., Konduru, N., Cortese, F., Bray, S., Gaxiola-Valdez, I., & Goodyear, B. (2014). Reduced intrinsic connectivity of amygdala in adults with major depressive disorder. *Frontiers in Psychiatry*, 2014, 5, 17. https://doi.org/10.3389/fpsyt.2014.00017

Rolls, E. T. (2016). A non-reward attractor theory of depression. *Neuroscience & Biobehavioral Reviews*, 68, 47–58. https://doi.org/10.1016/j.neubiorev.2016.05.007

Rolls, E. T. (2017). The roles of the orbitofrontal cortex via the habenula in non-reward and depression, and in the responses of serotonin and dopamine neurons. *Neuroscience & Biobehavioral Reviews*, 75, 331–334. https://doi.org/10.1016/j.neubiorev.2017.02.013

Rolls, E. T. (2014, 2014). *Emotion and decision-making explained*. Oxford University Press.

Rubinov, M., & Bullmore, E. (2013). Fledgling pathoconnectomics of psychiatric disorders. *Trends in Cognitive Sciences*, 17(12), 641–647. https://doi.org/10.1016/j.tics.2013.10.007

Sagliano, L., Magliacano, A., Parazzini, M., Fiocchi, S., Trojano, L., & Grossi, D. (2019). Modulating interoception by insula stimulation: A double-blinded tDCS study. *Neuroscience Letters*, 696, 108–113. https://doi.org/10.1016/j.neulet.2018.12.022

Sala-Llonch, R., Smith, S. M., Woolrich, M., & Duff, E. P. (2019). Spatial parcellations, spectral filtering, and connectivity measures in fMRI: Optimizing for discrimination. *Human Brain Mapping*, 40(2), 407–419. https://doi.org/10.1002/hbm.24381

Sankarasubramanian, V., Cunningham, D. A., Potter-Baker, K. A., Beall, E. B., Roelle, S. M., Varnerin, N. M., Machado, A. G., Jones, S. E., Lowe, M. J., & Plow, E. B. (2017). Transcranial direct current stimulation targeting primary motor versus dorsolateral prefrontal cortices: Proof-of-concept study investigating functional connectivity of thalamocortical networks specific to sensory-affective information processing. *Brain Connectivity*, 7, 182–196. https://doi.org/10.1089/brain.2016.0440

Shanahan, M. (2010). Metastable chimera states in community-structured oscillator networks. *Chaos: An Interdisciplinary Journal of Nonlinear Science*, *20*(1), 13108. https://doi.org/10.1063/1.3305451

Smith, S. M., Miller, K. L., Salimi-Khorshidi, G., Webster, M., Beckmann, C. F., Nichols, T. E., Ramsey, J. D., & Woolrich, M. W. (2011). Network modelling methods for FMRI. *NeuroImage*, *54*(2), 875–891. https://doi.org/10.1016/j.neuroimage.2010.08.063

Stark, E. A., Cabral, J., Riem, M. M. E., van IJzendoorn, M. H., Stein, A., & Kringelbach, M. L. (2019). The power of smiling: The adult brain networks underlying learned infant emotionality. *Cerebral Cortex*, *30*(4), 2019–2029. https://doi.org/10.1093/cercor/bhz219

Stephan, K. E., Weiskopf, N., Drysdale, P. M., Robinson, P. A., & Friston, K. J. (2007). Comparing hemodynamic models with DCM. *NeuroImage*, *38*(3), 387–401. https://doi.org/10.1016/j.neuroimage.2007.07.040

Tognoli, E., & Kelso, J. A. S. (2014). The metastable brain. *Neuron*, *81*(1), 35–48. https://doi.org/10.1016/j.neuron.2013.12.022

Uddin, L. Q., Nomi, J. S., Hébert-Seropian, B., Ghaziri, J., & Boucher, O. (2017). Structure and function of the human insula. *Journal of Clinical Neurophysiology*, *34*(4), 300–306. https://doi.org/10.1097/wnp.0000000000000377

Vann, S. D., Aggleton, J. P., & Maguire, E. A. (2009). What does the retrosplenial cortex do? *Nature Reviews Neuroscience*, *10*(11), 792–802. https://doi.org/10.1038/nrn2733

Wang, F., Jin, J., Wang, J., He, R., Li, K., Hu, X., Li, Y., & Zhu, Y. (2020). Association between olfactory function and inhibition of emotional competing distractors in major depressive disorder. *Scientific Reports*, *10*, 6322. https://doi.org/10.1038/s41598-020-63416-7

Wang, L., Wei, Q., Wang, C., Xu, J., Wang, K., Tian, Y., & Wang, J. (2020). Altered functional connectivity patterns of insular subregions in major depressive disorder after electroconvulsive therapy. *Brain Imaging and Behavior*, *14*(3), 753–761. https://doi.org/10.1007/s11682-018-0013-z

Wei, D., Wang, K., Meng, J., Zhuang, K., Chen, Q., Yan, W., Xie, P., & Qiu, J. (2019). The reductions in the subcallosal region cortical volume and surface area in major depressive disorder across the adult life span. *Psychological Medicine*, *1–9*, 422–430. https://doi.org/10.1017/S0033291719000230

Wong, K.-F., & Wang, X.-J. (2006). A recurrent network mechanism of time integration in perceptual decisions. *The Journal of Neuroscience: The Official Journal of the Society for Neuroscience*, *26*(4), 1314–1328. https://doi.org/10.1523/JNEUROSCI.3733-05.2006

Woo, C.-W., Chang, L. J., Lindquist, M. A., & Wager, T. D. (2017). Building better biomarkers: Brain models in translational neuroimaging. *Nature Neuroscience*, *20*(3), 365–377. https://doi.org/10.1038/nn.4478

World Health Organization (2008). *The global burden of disease: 2004 update*. World Health Organization. Retrieved from https://apps.who.int/iris/bitstream/handle/10665/43942/9789241563710_eng.pdf

Yan, C.-G., Chen, X., Li, L., Castellanos, F. X., Bai, T.-J., Bo, Q.-J., Cao, J., Chen, G. M., Chen, N. X., Chen, W., Cheng, C., Cheng, Y. Q., Cui, X. L., Duan, J., Fang, Y. R., Gong, Q. Y., Guo, W. B., Hou, Z. H., Hu, L., ... Zang, Y. F. (2019). Reduced default mode network functional connectivity in patients with recurrent major depressive disorder. *Proceedings of the National Academy of Sciences of the United States of America*, *116*(18), 9078–9083. https://doi.org/10.1073/pnas.1900390116

Yan, C.-G., Wang, X.-D., Zuo, X.-N., & Zang, Y.-F. (2016). Dpabi: Data Processing & Analysis for (resting-state) brain imaging. *Neuroinformatics*, *14*(3), 339–351. https://doi.org/10.1007/s12021-016-9299-4

Yang, H., Chen, X., Chen, Z.-B., Li, L., Li, X.-Y., Castellanos, F. X., Bai, T. J., Bo, Q. J., Cao, J., Chang, Z. K., Chen, G. M., Chen, N. X., Chen, W., Cheng, C., Cheng, Y. Q., Cui, X. L., Duan, J., Fang, Y., Gong, Q. Y., ... Yan, C. G. (2021). Disrupted intrinsic functional brain topology in patients with major depressive disorder. *Molecular Psychiatry*, *26*(12), 7363–7371. https://doi.org/10.1038/s41380-021-01247-2

Zhang, F.-F., Peng, W., Sweeney, J. A., Jia, Z.-Y., & Gong, Q.-Y. (2018). Brain structure alterations in depression: Psychoradiological evidence. *CNS Neuroscience & Therapeutics*, *24*(11), 994–1003. https://doi.org/10.1111/cns.12835

Zhuo, C., Li, G., Lin, X., Jiang, D., Xu, Y., Tian, H., Wang, W., & Song, X. (2019). The rise and fall of MRI studies in major depressive disorder. *Translational Psychiatry*, *9*(1), 335. https://doi.org/10.1038/s41398-019-0680-6